

NEW SUBSTANCES, MATERIALS,
AND COATINGS

Enhanced Adhesion and Corrosion Properties of Boron Doped Bioceramic Coated 316L Implants

M. E. Aksoy^a, B. Aksakal^{b, *, **}, N. Aslan^{c, d}, and B. Dikici^e

^a Institute of Post Graduate Education, Munzur University, Tunceli, 62000 Turkey

^b Department of Metallurgical and Materials, Yildiz Technical University, Istanbul, 34220 Turkey

^c Department of Metallurgical and Materials, Munzur University, Tunceli, 62000 Turkey

^d Munzur University, Rare Earth Elements Application and Research Center, Tunceli, Turkey

^e Department of Metallurgical and Materials Engineering, Ataturk University, Erzurum, 25240 Turkey

*e-mail: baksakal@yildiz.edu.tr

**e-mail: baksakal2@gmail.com

Received December 24, 2020; revised April 1, 2021; accepted May 10, 2021

Abstract—In order to provide an effective prevention to 316L implants, a synthesized bioceramic was coated by using electrophoretic deposition (EPD). The effect of boron addition into hydroxyapatite (HA) on surface morphology, adhesion and corrosion resistance of the implant has been examined. Boron doped HA (B–HA) was synthesized by a simple chemical acid–base method with 5, 10, and 15 wt % boron additions to coat on 316L implants. The synthesized B–HA was coated on the substrates and the coated surfaces with and without B additions. Sintering took place at different temperatures and sintering rates. The coatings were characterized by X-ray diffractometer (XRD), Fourier transform infrared spectroscopy (FT–IR) and scanning electron microscope (SEM). Furthermore, adhesion and in vitro corrosion tests were conducted. The influence of boron additions on adhesion and corrosion resistance of 316L have been revealed for the coated substrates at different B additions. It was shown that boron addition increased the adhesion and corrosion resistance of the bioceramic coatings. Furthermore, the sintering effect on adhesion was also evaluated and the highest adhesion as 25.8 MPa has been reached at 750°C for 90 s and 5°C min^{−1} sintering conditions. It was found that using iodine as EPD dispersant has increased the charging ability of the B–HA powders in the suspension and hence eased deposition rate. The study revealed that boron-containing hydroxyapatite coatings can provide crack-free surfaces that providing high adhesion and hence increase the corrosion resistance of metallic implants. Through the results, it was also shown that the network between powders was improved and hence adhesion was increased with increasing B addition.

Keywords: 316L implant, bioceramic coating, boron, hydroxyapatite, electrophoretic deposition

DOI: 10.1134/S2070205121050026

1. INTRODUCTION

Biomaterials implanted used as substitutes in hard tissues are expected to have properties such as good strength, biocompatibility, fixation, corrosion resistance. Such substitute orthopaedic materials are subjected to various dynamic loads, stresses and a corrosive environment during the daily activities of the body. Therefore a good osteointegration between the implant and bone is required also providing the implant material should have high corrosion resistance into the body fluid [1–3]. The corrosion resistance and biocompatibility of 316L is weaker than Ti and Co–Cr–Mo alloys in a live body environment. These problems can be minimized by bioactive ceramic coatings on metallic implants used in orthopedics. The main purpose of surface coating in metallic implants is to eliminate possible disadvantages that

cause allergic tissue reactions such as corrosion and releasing metal ions [4–6]. Hydroxyapatite (HA) is a bioactive and nontoxic biomaterial that is highly similar to human bone and allows the bone to develop and thanks to its porous structure, which supports cell growth, cell proliferation, and tissue development [7–10]. Although it is heavily used in biomedical applications, HA has low mechanical strength when used in load-bearing applications and causes adhesion problems when used as coated implants. Therefore, the HA materials were used with some reinforcing materials especially in metallic surface coatings to improve such properties [11–16]. It has been reported that boron (B) and its compounds play an important role in bone healing and osteogenesis processes in boron-doped HA studies where the HA structure was reinforced with boron [17, 18]. Also, other studies have

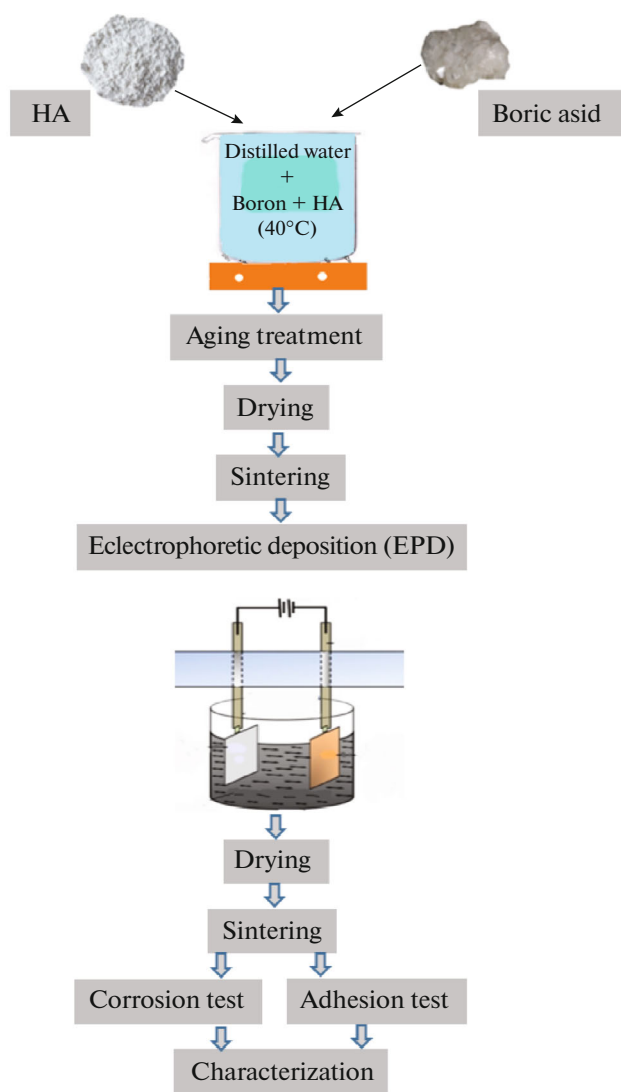


Fig. 1. Flowchart of experimental procedures.

shown that healthy bones contain more boron than rheumatoid arthritis bones [19, 20].

The electrophoretic deposition method (EPD) is a multifunctional and advantageous coating method that allows bioactive and homogeneous coating of even complex implant parts, providing conditions such as low cost, easy installation, and control of coating thickness [21–23]. For such purposes, Wennerberg et al. [24] tried to reveal the adhesion, corrosion, and bioactivity properties of chitosan/h-BN/titanium oxide composite coatings on 316L substrates by using the EPD method. The study showed that the composite coating improved the adhesion and corrosion properties compared to uncoated-316L, did not show bioactive properties, but may be suitable as antibacterial coatings. Tozar and Karahan [25] carried out a hydroxyapatite/chitosan/collagen/h-BN bioceramic coatings on Ti6Al4V substrates and it was reported that

the corrosion resistance, mechanical and tribological properties of the substrates improved as the hexagonal boron nitride (h-BN) addition increased. Göncü et al. [26] coated Ti substrates with nano h-BN and nano HA using the EPD method and claimed that the h-BN in the suspension did not have any significant impact on the coating thickness and the HA morphology of the porous coating. The literature also includes the studies synthesizing calcium-phosphate composite powders doped with boron and boron derivatives and revealing their morphological properties through various methods. As can be understood from previous literature that B–HA composite powder productions have been studied in general, and mostly h-BN derivatives have been used as a coating.

Unlike the literature, in this study, HA powders doped at varying amounts (5, 10, and 15 wt %) of B and B–HA bioceramics were synthesized using a simple acid–base technique, the powders were ground and reduced to a suitable powder size after sintering process, and finally the EPD coating was performed on 316L alloy at different charging times. The effects of the bioceramic coatings on those of structural properties, morphology, optimum sintering conditions, coating thickness, adhesion, corrosion resistance, and B–HA addition ratios were examined extensively and comparatively.

2. EXPERIMENTAL

2.1. Materials

316L SS sheet metallic substrates were used. The 316L SS alloys were procured as $1 \times 250 \times 250$ mm sheets (ASTM A240/A240M). The sheet plates were cut off into 10×15 mm samples and their surfaces were blasted by silicon dioxide (SiO_2) sand ($300 \mu\text{m}$) beads. It has been reported in the literature that some surface treatments, such as blasting, chemical and laser treatment have positive effects on adhesion, [13, 14]. As specimen pre-treatments, Ultrasonic cleaning (Bandelin Sonorex, RK31H) procedure was applied to the samples after sandblasting performed on the metallic substrate samples. Experiments were repeated three times and the calculated data were presented statistically as averagely with the standard error values (OriginPro 2015 SR2, Northampton, MA). The *t*-test was used to determine the significant differences between groups and a *p*-value less than 0.05 was accepted as statistically significant.

2.2. Synthesizing of Boron-Doped Bioceramic (B–HA)

Boron doped HA (B–HA) powders were produced using a simple chemical “acid–base” method for obtaining bioceramic coatings on 316L implant materials. The HA ($<25 \mu\text{m}$, Nanograph, Turkey) with 99% purity and H_3BO_3 ($<25 \mu\text{m}$, Merck) were used for obtaining B–HA bioceramic coatings in this study.

Table 1. 316L Coating times and compositions of the coatings with sample ID

Coating time (s)	only-HA	5 wt % B–HA	10 wt % B–HA	15 wt % B–HA
60	L ₁	L ₄	L ₇	L ₁₀
90	L ₂	L ₅	L ₈	L ₁₁
120	L ₃	L ₆	L ₉	L ₁₂

The HA-based B-doped bioceramic was synthesized at three different ratios: 5, 10, and 15 wt %. Firstly, H₃BO₃ was added to the distilled water in the magnetic mixer at a constant temperature of 40°C, and after dissolution, HA was added into the sol as given in experimental flow chart (Fig. 1). Following, the aging process was performed by adding sodium hydroxide (NaOH, Merck) to keep the pH value at 7.40. The aging process was performed by mixing for 12 h in the magnetic mixer and 7 min in the homogenizer, respectively. After aging, the samples were left in a drying furnace for 24 h to dry at 130°C. Finally, it was sintered for 2 h at 10°C min⁻¹ heating-cooling rate. Boron powders were then manually ground in a ceramic mortar to the average particle size of 25 µm.

X-ray diffraction (Rigaku–MiniFlex 600) and FT-IR analyses (Jasco 6700) were performed to characterize the presence of boron in B–HA bioceramic powders. Precision scales (Radwag PS600.R2), magnetic stirrer (Mtops HS12, 1500 rpm), ultrasonic homogenizer (Sonic VC 505, 750 W), drying furnace (Binder ED23, 300°C), and atmosphere-controlled/vacuum horizontal tube furnace (MSE, 1500°C) were used through the surface coating operations.

2.3. Suspension Preparation for EPD Process

N,N-Dimethylformamide (DMF), ethanol (Merck), and suspension variables in the coating suspension were prepared in four different groups as the only-HA, 5, 10, and 15 wt % boron-doped coating. The suspensions were homogenized in a magnetic stirrer for 25 min and in an ultrasonic homogenizer for 5 min at 20 kHz. It was reported that there was an increase in electrical conductivity when the iodine was added to the EPD suspension [34]. During the EPD coating procedures, Iodine was added into all suspensions to increase the electrical conductivity (charging ability) of non-conducting particles (HA and B) after the homogenizing process.

2.4. EPD Process and Sintering

Stainless steel plates at anode and cathode were used coupled with a DC power source in the EPD processes. The substrates fixed to the cathode electrode and substrates were coated with the prepared only-HA, 5, 10, and 15 wt % B-doped suspensions at 150 V with a 10 mm fixed electrode distance for 60, 90, and 120 s deposition times, respectively. Table 1 shows the percentage of weight ratios and coating times of the

316L samples coated with the EPD process. Hereafter, the coatings are referred to as L_{*n*} for easy expression according to coating time and B ratio in the coatings. For example, considering the table, the code L₁₀ means that the surface of the 316L sample was coated with 15 wt % B–HA bioceramic powder for a deposition time of 60 s. After the coating process, the samples were left to dry for 24 h under room conditions. All samples were sintered at the optimal sintering parameters (750°C, 75 min) in a vacuum environment with a heating and cooling rate of 10°C min⁻¹, after predrying for 240 min at 130°C. After sintering, all samples were stored in a desiccator for characterization, analysis, adhesion and corrosion tests.

2.5. Adhesion Tests

Adhesions of the bioceramic coatings on metallic sample surfaces were tested by the ISO 13779-4 standard. To measure the adhesions of the EPD coatings on the metallic implant surfaces, pull-out tests were performed by mounting a specially designed and manufactured die-apparatus on the jaws of the tensile test machine (Shimadzu, 100kN). The DP420 (3M) was used as an adhesive and uncoated/coated 316L rods having 8 mm in diameter whose forehead cross sections correspond to 50 mm² were bonded. The glued adhesion sample couple (coated/uncoated rods) was placed in the previously designed and placed on upper and lower jaws at a 90° angle to the surface axis. The reference rods' weights were used and care was taken to prevent overflow and axial leaks. After placing, the final drying process was applied for 4 h at 130°C in a drying furnace after keeping for 12 h under room conditions (25°C) to dry the adhesive. Adhesion tests were performed with a tensile rate of 1 mm min⁻¹. The rupture force obtained from the pull-out tests were converted to adhesion by dividing the cross sectional area. At least three samples were tested for each coating group and mean results were determined.

2.6. In Vitro Corrosion Tests

Corrosion tests were performed with a potentiostat/galvanostat (Gamry, PCI14/750) in the simulated body fluid (SBF) at 37°C and the three electrode technique was used during the polarization tests. A silver/silver chloride electrode (Ag/AgCl) and platinum (Pt) wire and coated samples were used as reference, counter, and working electrodes, respectively. The SBF was pre-

Table 2. Similarity of blood plasma to simulated body fluid (SBF) via ion concentration for 10^{-3} moles

Ion	Blood plasma	SBF
Na ⁺	142	142
K ⁺	5	5
Mg ²⁺	1.5	1.5
Ca ²⁺	2.5	2.5
Cl ⁻	103	147.8
HCO ₃ ⁻	27	4.2
HPO ₄ ²⁻	1	1
SO ₄ ²⁻	0.5	0.5
pH	7.2–7.4	7.40

pared according to the Kokubo's protocol [27]. The reason for using SBF in corrosion testing is that it has similar values to ion concentrations in blood plasma. Table 2 shows the ion concentrations of blood plasma and the SBF liquid as comparatively. Through the tests, first, samples were immersed into the SBF until obtaining a steady-state open circuit potential (OCP). After reaching equilibrium, the potentiodynamic scanning (PDS) test got started at the cathodic overpotential at a rate of 1 mV s^{-1} and the scan has been stopped when the specimens reached the anodic overpotential at 0.2 V. Electrochemical data were calculated by using the Tafel method from the PDS curves. The corrosion current density (I_{corr}) and corrosion potential (E_{corr}) values were calculated by the intersection of linear portions of the anodic (β_a) and cathodic (β_c) Tafel slopes [28, 32]. The corrosion rates and polarization resistances of the samples were calculated together with Tafel parameters by using Gamry Echem Analyst software.

2.7. SEM-EDX and XRD Analysis

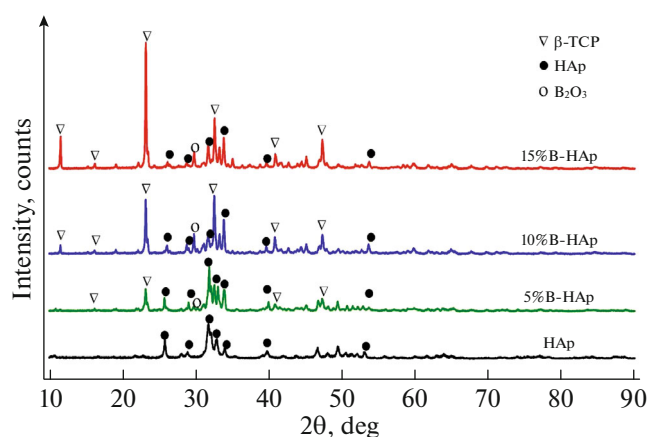
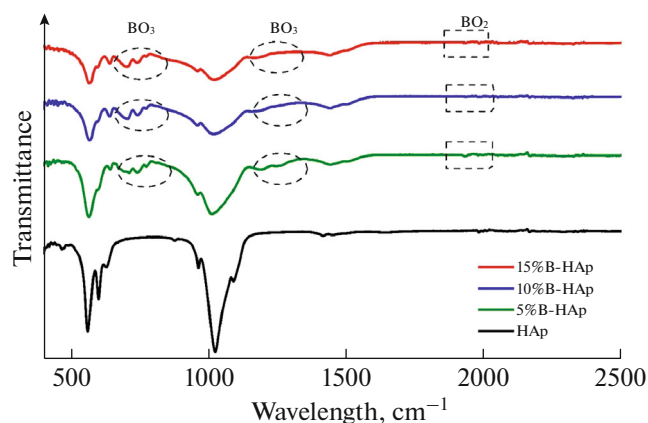
The surface morphologies of the coated samples were characterized by a scanning electron microscopy (SEM, Hitachi SU3500) and the spectra (EDX-Oxford Inca) of the scanned zones were determined. The XRD analyses (Rigaku, MiniFlex-600) were conducted at a wavelength of 1.5406 \AA between 10 and 90° with a step speed of 0.02° .

3. RESULTS

To show the impacts of the different boron additions (wt %) into hydroxyapatite, the comparative presentations of morphological, adhesion, corrosion and of the EPD deposited surfaces were shown as microscopic, spectrum and graphical views. The characterization of powder morphology of the synthesized B reinforced HA bioceramic (B-HA) was presented in related sections. Changes on the surfaces and adhesion properties of the coated samples subjected to cor-

rosion tests were presented in a comparison manner as before and after corrosion.

FT-IR and XRD analyses were performed after the hydroxyapatite powders doped with 5, 10, and 15 wt % B were sintered at sintering conditions at 750°C for 2 h.


Fig. 2. XRD analysis of only-HA and 5, 10, and 15 wt % B-HA powders.

Fig. 3. FT-IR analysis of only-HA and 5, 10, and 15 wt % B-HA powders.

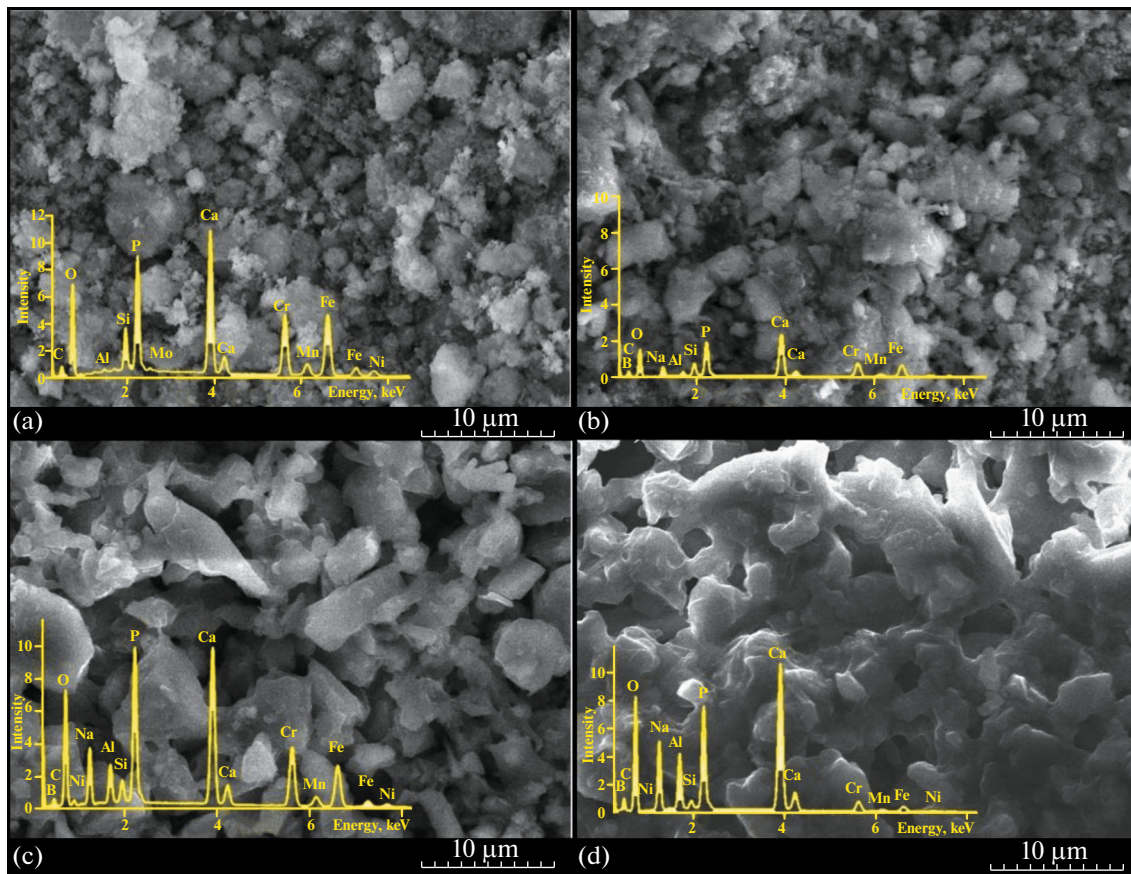


Fig. 4. SEM images and EDS spectrums of (a) only HA (L_2) and (b) 5 (L_5), (c) 10 (L_7) and (d) 15 (L_{10}) wt % B–HA coatings.

Figure 2 shows the XRD spectra of the boron-doped (5, 10, and 15 wt %) bioceramics and the only-HA powders. The resulting peaks in the spectra indicate that the boron contribution [29] partially disrupted the structure of HA and transformed to TCP (tricalcium phosphate). The surfaces of substrates were coated by the synthesized bioceramic for different B additions. Boron characterization within the bioceramic structures is also shown by FT-IR analyses. Figure 3 shows the comparison of FT-IR spectra of the only-HA and 5, 10, 15 wt % boron-doped HA powders. Figures 4a–4d shows the SEM surface images of the 316L, only-HA, and 5, 10, and 15 wt % B–HA bioceramic coating groups. Table 3 shows the coating thickness values; the highest and lowest thickness values were measured in the L_{12} samples ($74.7 \pm 3.5 \mu\text{m}$) and the L_4 samples ($25.9 \pm 1.5 \mu\text{m}$), respectively. As can be seen in Fig. 5, the coating thickness of the L_1 , L_2 , and L_3 samples coated with only-HA increased with increasing coating times.

The bioceramic powders coated on the unit area (cm^2) for groups of the only-HA, and 5, 10, and 15 wt % B–HA coatings applied to the 316L SS substrates for 60, 90, and 120 s. Pull-out tests were performed to determine the adhesion on the 316L substrates and the

coating interfaces. The most important factor affecting the adhesion of coatings is the coating-sample merging interface. It was shown that sintering conditions e.g both sintering temperature and speed have also significant effect on adhesion. Figure 6 shows the effects of sintering processes performed at 3, 5 and

Table 3. Coating thicknesses and their adhesion strengths of the coatings

ID	Coating thickness, μm	Adhesion, MPa
L_1	26.1 ± 0.3	19.7 ± 1.2
L_2	31.1 ± 4.2	17.2 ± 1.6
L_3	33.6 ± 3.9	16.4 ± 0.4
L_4	25.9 ± 1.5	20 ± 2.0
L_5	28.8 ± 1.1	22.1 ± 1.5
L_6	34 ± 5.8	21.3 ± 0.6
L_7	47 ± 1.6	18.8 ± 0.5
L_8	53.8 ± 1	20.5 ± 1.6
L_9	61.8 ± 3.4	25.7 ± 1.1
L_{10}	63.3 ± 8.8	22.1 ± 1.1
L_{11}	68.2 ± 2.1	25.8 ± 1.3
L_{12}	74.7 ± 3.5	22.9 ± 1.2

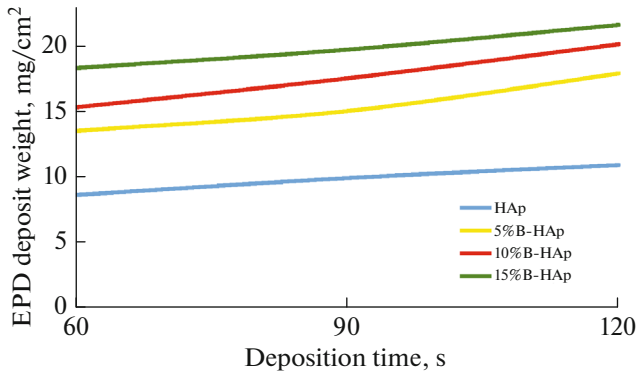


Fig. 5. Variation of the EPD deposition weight with coating time.

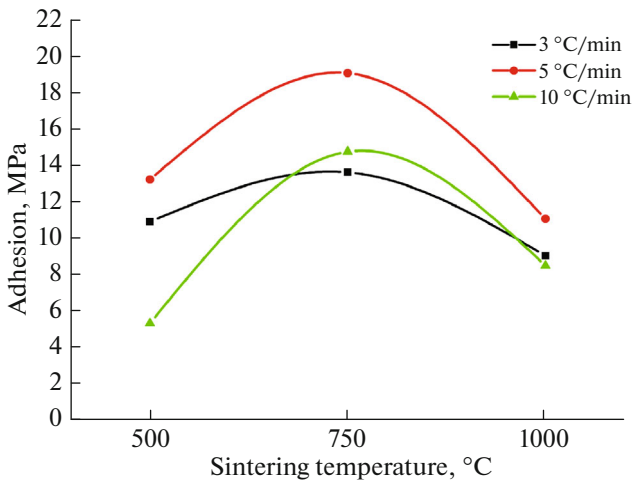


Fig. 6. The effect of sintering temperatures and speeds on adhesion.

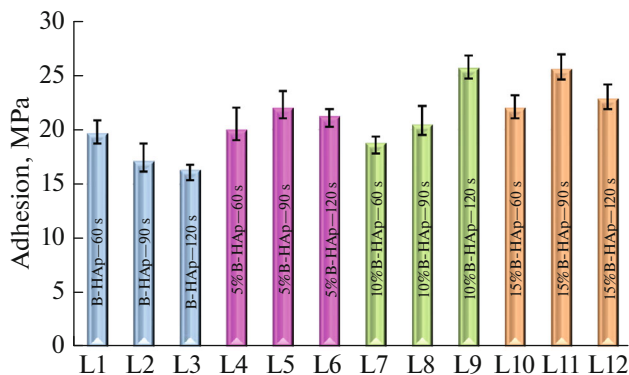


Fig. 7. Changes in adhesion with B addition and deposition time of the coated sample groups.

10°C min⁻¹ heating and cooling speeds with 500, 750, 1000°C temperatures on adhesion of bioceramic coated groups.

The main goal of the study was to achieve a bioceramic powder synthesizing with various B additions and provide a protective implant surfaces against corrosion. To show such effect, in vitro corrosion tests have been conducted to those uncoated and B-HA coated substrates. The results are presented via the steady-state open circuit potential-OCP and potentiodynamic scanning-PDS curves in Figs. 8 and 9, respectively. Figures 10a–10d show the XRD analyses of the uncoated before (a) and after corrosion (b); and the only-HA coated 316L samples pre-corrosion (c) and post corrosion (d). As observed from the spectra, there are only 316L peaks before corrosion while the 316L peaks decreased and CrO₃ oxide structures were formed in certain zones after corrosion. This oxide structure supported the destruction that occurred on the surface of the uncoated 316L sample after corrosion.

SEM surface images of the L₅ samples coated with 5 wt % boron-doped HA and the pre-corrosion morphology of the EDX spectra are given in Fig. 4b while the post-corrosion morphology is given in Fig. 11b. The obtained surface was crack-free and low-porosity before corrosion, whereas an increase was observed in porosity and cracks on the surface after corrosion.

Pre-corrosion (Fig. 4c) and post-corrosion (Fig. 11c) SEM surface images and EDX spectra of the coated surface morphology of the L₇ are given. The pre-corrosion (Fig. 4d) and post-corrosion (Fig. 11d) SEM images and EDX spectra of the L₁₀ samples in the 15 wt % B-HA bioceramic coatings are given. The surface morphology of the coating revealed that the bonds between the grains slightly weakened and the porosity increased after corrosion.

4. DISCUSSION

4.1. Characterization of Bioceramic Synthesis

The presence of boron in the currently synthesized bioceramic was shown in Fig. 2. From the spectra, it was determined that there exist HA and partially TCP peaks in the synthesized bioceramic besides B additive. It was pointed out in a previous study that increased boron addition into HA caused some degradation in the structure after sintering and increased boron rate caused an increase TCP formation [26, 31]. It was observed that the phases formed as shown in XRD spectra of the boron-doped HA composite were different from those found in the study conducted by Ternane et al. [18]. From the peaks, no unwanted phases such as CaO was observed, peak intensity increased with increasing boron addition and the crystallization rate was very high. B₂O₃ structures identified in 2θ range at 29.9° in XRD analyses coincide with the presence of B₂O₃ structures identified in XRD results (2θ = 29.9°) in the study conducted by

Khoshima et al. [30] in which the B_2O_3 -HA bioceramics were synthesized in different proportions.

As given in Fig. 3, FT-IR analysis also proved the existence of such structures in the synthesized bioceramic powder to be coated on 316L substrates. The obtained peak values of BO_3^{3-} and BO_2^- structures in the FT-IR analyses of the bioceramic powders may result from the inclusion of B in the aimed bioceramic structure. B-doped HA synthesized studies have determined that BO_3^{3-} structure peaks were observed at 744, 770, 783 and 1304, 1254, 1204 cm^{-1} wavelengths, and BO_2^- structure peaks in 1993 and 2000 cm^{-1} wavelength [18, 21, 32]. The peaks of BO_3^{3-} and BO_2^- structures obtained in this study are consistent with the findings reported in the literature.

4.2. EPD Coating

The main purpose of coating metallic implants with materials such as bioceramic is to improve both corrosive protection and implant-tissue interactions and so fixation. The adequate adhesion between the coating and the implant and the formation of the coating-tissue interaction provide a high level of implant fixation. The porous structure is preferred for coating as it increases the bonding ability between the implant and the tissue in medical applications. For this reason, the fact that the coatings have porous morphology in the coating-tissue interaction provides an advantage for the tissue growth.

By considering these points, SEM views of the coated substrates are given in Figs. 4a–4d. Interactions between the powder grains can be clearly seen in the only-HA (a), 5 (b), 10 (c), and 15 wt % B–HA (d) bioceramic coatings. This indicates that good bonding and increased bonding strength between the powders achieved by sintering have a positive impact on adhesions, and it helps to increase corrosion resistance. The best inter-powder bonding among the bioceramic coatings applied to 316L substrates was found to be belongs to the 15 wt % B–HA coating group (Fig. 4d).

Figure 5 shows the variation of deposit weights (mg) with deposition time and B (wt %) additions. Through the groups of 5, 10, and 15 wt % B–HA, it was determined that the increased B-additive ratio affected the increase in coating thickness. However, the coating thickness of the 5 wt % boron-doped HA (L_4 , L_5 , and L_6) decreased at same EPD time parameters compared to the only-HA coatings (L_1 , L_2 , and L_3). This decrease may be attributed to the low amount of charged 5 wt % B–HA bioceramic coatings due to the difference in charged particle size in the EPD deposition suspension and inability to transport large particle powders to the cathode because they cannot be charged and move easily. It was observed that the highest deposition has been found in the 15 wt % B–HA bioceramic

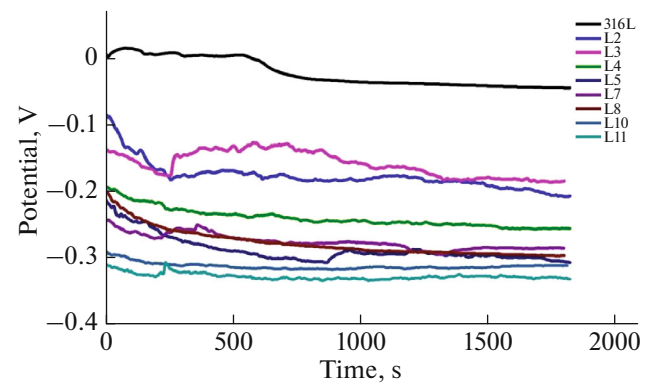


Fig. 8. Open circuit potential (E_{ocp}) curves of the coated samples in SBF.

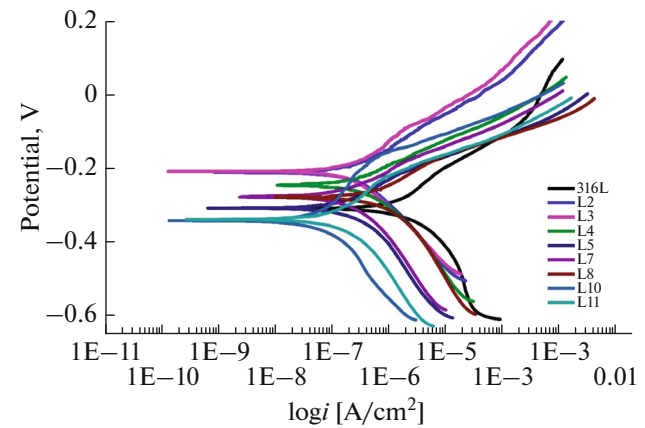


Fig. 9. Potentiodynamic scanning (PDS) curves of the coated samples in SBF.

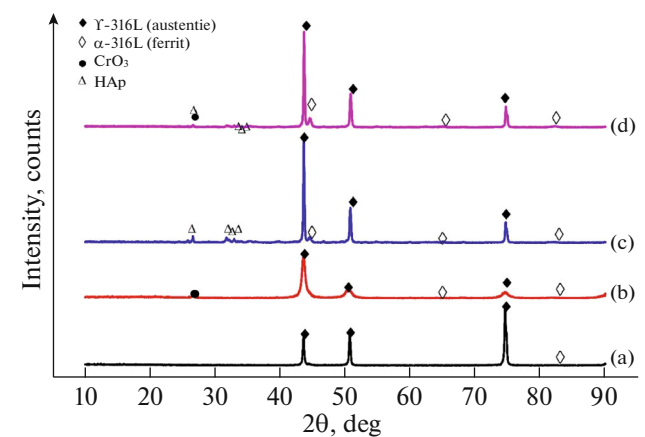


Fig. 10. XRD analysis of the uncoated (a) pre-corrosion and (b) post-corrosion; and only-HA coated 316L samples (c) pre-corrosion and (d) post-corrosion.

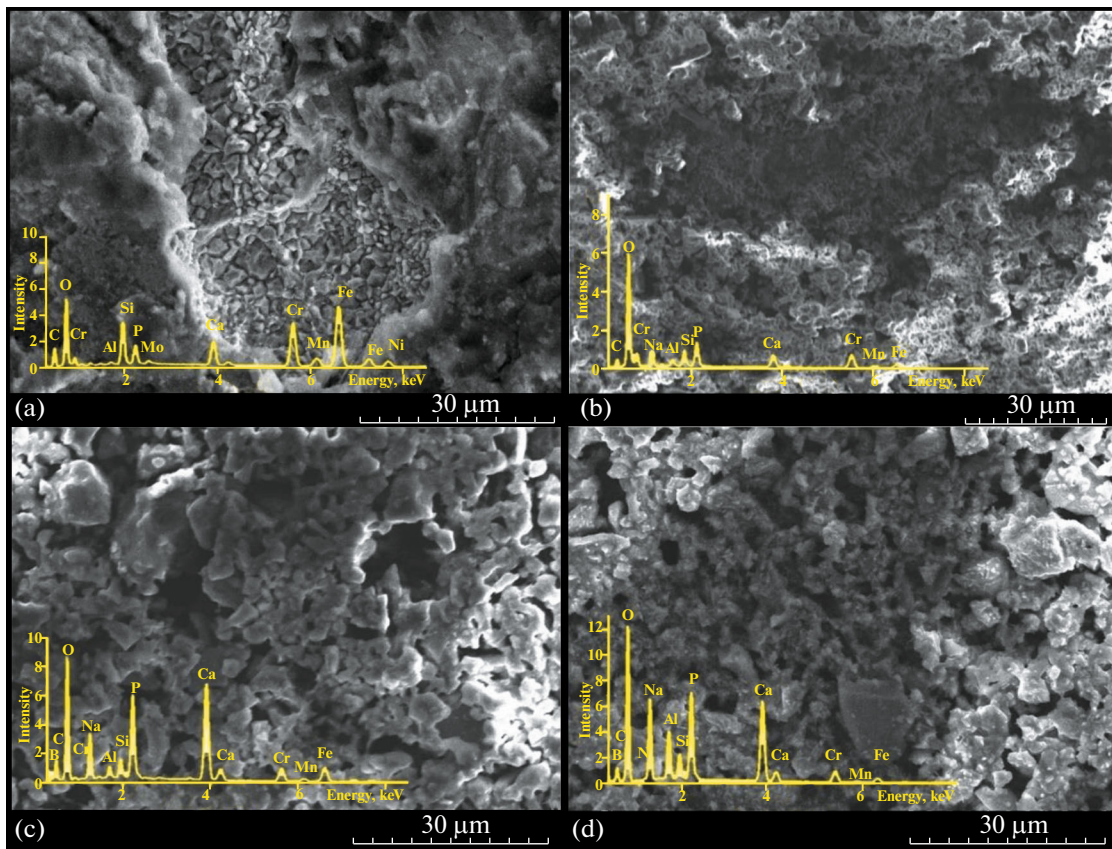


Fig. 11. SEM images and EDS spectrums after corrosion tests in SBF of (a) only HA and (b) 5 wt % B, (c) 10 wt % B and (d) 15 wt % B of B–HA bioceramic coated samples.

coatings while the lowest deposition took place in the only-HA coatings, and the weights per unit area increased in all coatings as the EPD charging times increased. This may be because the increased B ratio increased the conductivity of the charged particles in the EPD coating suspension and that causing more deposition on the substrate surfaces. The amount of coating accumulated per unit area on the substrate surface decreases depending on the increasing charging time in the EPD deposition and causes a hesitance in very long coating times [11, 14, 27]. The main reason for this may be the fact that the thickness of the coating, which increases depending on EPD time, forms an isolated layer by weakening the conductivity of the metallic substrate surface. The results in Fig. 5 indicate that the coating which accumulated per unit area increased in parallel with the increasing coating time and the coating time was not enough for the coating to become stable.

4.3. Adhesion

Adhesion tests have been executed to show the effect of sintering temperature and heating/cooling rate on corrosion and adhesion between the coating and substrate-316L. The mean adhesion values obtained

from the tests are tabulated in Table 3 and comparative adhesion test results in Fig. 6. During the pull-out tests, it was observed that the coating could be easily peeled off the surface due to insufficient interface strength at low sintering temperature (500°C) and therefore the adhesions were found to be low. Similarly, most probably the existence of different thermal expansions of the biocomposite and metallic sample at higher sintering temperatures higher than 750°C e.g. at 1000°C also caused a decrease in adhesions. The oxide layer formed on the coating and metallic substrate interface during the sintering operation performed at 1000°C and 3, 5, and 10°C min⁻¹ sintering rates caused the adhesions to be as low as 9.03 ± 0.9 , 11.06 ± 1.32 , and 8.49 ± 1.7 MPa, respectively. As can be seen from the Fig. 6, the highest adhesions (13.61 ± 2.3 , 19.06 ± 1.2 , and 14.75 ± 1.02) were determined at 750°C sintering temperature.

Comparative histogram graphs of the adhesion of only-HA, and 5, 10, and 15 wt % B–HA groups are given in Fig. 7. The increased bioceramic coating thickness on the metallic surface due to coating time in only-HA coatings applied to the L₁, L₂, and L₃ samples decreased the adhesion. In this case, the adhesion reached the highest level in the 120 s coating time as

Table 4. Corrosion parameters calculated from PDS curves of the coatings

ID	E_{ocp} , mV	E_{corr} , mV	I_{corr} , nA cm ⁻²	Corr. rate, mpy	R_p , $\times 10^3$ ohms cm ²
uncoated 316 L	-45	-167	249	0.106	113
L ₁	-242	-247	291	0.125	100
L ₂	-205	-210	252	0.108	121
L ₃	-187	-208	223	0.095	72
L ₄	-261	-245	302	0.129	130
L ₅	-306	-307	192	0.082	60
L ₆	-286	-273	387	0.166	129
L ₇	-284	-276	196	0.084	37
L ₈	-296	-278	724	0.311	10
L ₉	-308	-291	288	0.123	49
L ₁₀	-311	-341	86	0.037	228
L ₁₁	-328	-338	134	0.057	114
L ₁₂	-337	-343	280	0.120	113

the thickness increased in the 10 wt % B–HA coatings. The best strength among the samples with 5 and 15 wt % B–HA coating was obtained in the samples that coated for 90 s. The highest adhesion was found to be 25.8 MPa which belonged to the L₉ sample group that coated with 15 wt % B–HA with a coating thickness of 68.2 μ m. Compared to our work, lower values e.g., 15 MPa was found in a similar work executed by Wei et al. [33].

4.4. Corrosion

Figure 8 shows the open circuit potential (E_{ocp}) curves of the 316L samples applied in the SBF electrolytes in a comparative manner. Long enough immersion times were given for all samples to reach a stable state. The samples in L₁₀ and L₁₁ groups became stable in the shortest periods. The shift of the E_{ocp} value to more anodic potentials compared to the initial potentials depending on time indicates the presence of local corrosion on the surface [1, 10]. Figure 9 shows the potentiodynamic scanning (PDS) curves of the bioceramic coatings in the SBF electrolytes comparatively. The correlation between the potential and the current density logarithm reveals the corrosion potential (E_{corr}) and corrosion current (I_{corr}) values in addition to providing information about anodic and cathodic reactions taking place during the corrosion experiment through the Tafel method. Table 4 shows the measured values of E_{ocp} , E_{corr} , I_{corr} , β_a , β_c , corrosion rate, and corrosion resistance (R_p). From Table 4, as in L10 group, the fact that providing the I_{corr} value is low and the E_{corr} value is close to zero indicates to high corrosion resistance.

Based on PDS curves, it is observed that the potential increases and the current decreases in the bioceramic coatings applied to all 316L substrates. In this case, it was revealed that activation-controlled corrosion occurs in coatings, and therefore it may be more appropriate to compare I_{corr} values to determine corrosion trends and resistances [9, 20]. Such I_{corr} values for the uncoated 316L samples were calculated as 249 nA cm⁻² and -167 mV, respectively (Table 4). Since the fact that the I_{corr} values of coatings made with only-HA (L₁, L₂) were higher than the values of the uncoated samples indicates that the corrosion resistance decreased. The corrosion resistances of the L₅ sample in the 5 wt % boron-doped HA group, L₇ sample in the 10 wt % B–HA group, L₁₀, and L₁₁ samples in the 15 wt % B–HA groups increased.

When the SEM surface images shown in Fig 4a, and EDX spectra of the 316L substrate sample (L₂) coated with only-HA for 90s before and after corrosion given in Fig. 11a are considered, the post-corrosion images revealed that the corrosion environment weakened the coating and reaching the substrate material. According to the findings obtained from the EDX spectra, an increase was detected in the Fe–Ni–Mo peak intensities while the Ca–P peak intensities decreased. The EDX and XRD analyses revealed the corrosion formation on the surfaces and loss of effect of the coating (Ca and P ratios). The pre-corrosion and post-corrosion XRD analyses shown in Figs. 10c–10d verify that the HA peak intensities significantly decreased in the 2 θ range. Moreover, ferrite phases (α -316L) were formed at 2 θ = 44.5, 65, and 82.3° depending on the 750°C sintering temperature.

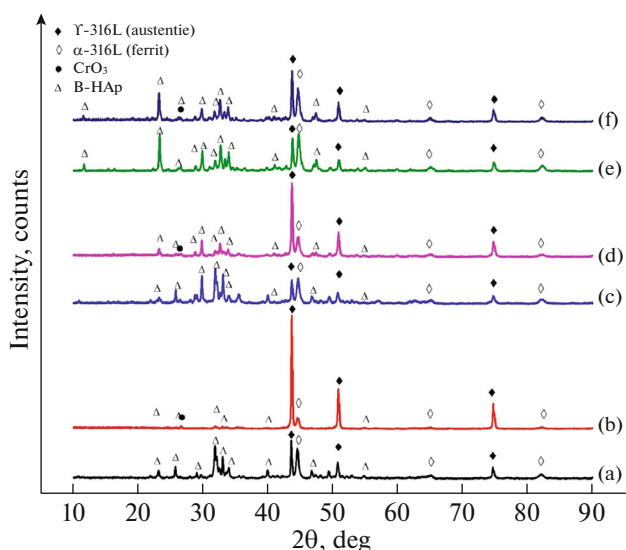


Fig. 12. XRD analysis of before and after corrosion tests for 5 wt % B (a–b), 10 wt % B (c–d) and 15 wt % B (e–f) of B–HA bioceramic coated samples.

Failures occurred where the grains were weakly tied to each other due to the impact of the corrosion environment. As a result, the corrosion caused damages by reaching to the surface of the metallic substrate. The Na element identified in the EDX spectra of 5 wt % B–HA coatings (Fig. 11b) penetrated the structure from the NaOH addition used as a pH regulator while synthesizing boron-doped powders. According to the EDX analyses, the Ca–P–B ratios in the coating decreased after the damage caused by corrosion. It was observed that the coating was damaged locally by reaching the metallic surface through the pores. The increased Fe–Cr–O ratios in the post-corrosion EDX analyses, the CrO_3 compound observed in the XRD analyses given in Figs. 12a–12b, and the increase in the α -316L and γ -316L peak intensities of the 316L substrate confirm the damage caused by the corrosion on the substrate.

When the surface images of the L_7 samples were examined, no serious damage is observed on the coating surfaces after corrosion. According to the EDX analyses obtained from the 10 wt % boron-doped HA bioceramic coating of the L_7 sample (Fig. 11c), a decrease was detected in Ca–P ratios, but a decrease was observed at lower rates compared to the only-HA and 5 wt % B–HA coatings. Furthermore, the increase in the boron ratio means that it was not affected in the corrosion environment and remained bonded with HA in the bioceramic structure. It is understood that the boron usage as an additive in the 10 wt % B–HA bioceramic coatings increased the corrosion resistance. This is confirmed by the little decreases in the 10 wt % B–HA peak intensities after corrosion as shown in the XRD analyses given in

Figs. 12c–12d. However, the CrO_3 peak was observed at $2\theta = 27^\circ$ where the corrosion impact reached the metallic substrate surface in the L_7 coatings, and the increases in the γ -316L ($2\theta = 44.51, 75^\circ$) peak intensities confirm that the corrosion impact reached the metallic surface and caused corrosive damage.

There was a decrease in the Ca–P–B ratios while the Fe–Cr–Mn ratios also increased after corrosion. A decrease in the ratio of the coating material (Ca–P–B) after corrosion destruction indicates that the coating on the metallic surface was weakened. Figures 12e–12f show the pre-corrosion (e) and post-corrosion (f) XRD analyses of the N_{10} sample where the 316L stainless steel substrate was coated by bioceramic coating of 15 wt % B–HA. According to XRD and EDX analyses, a slight decrease was detected in the peak intensities for the 15 wt % B–HA bioceramic coating group. While not like other groups, at 2θ : 11.50, 23.5, 30, 32.50, 34, and 47.40, the 316L peaks (α -316L and γ -316L) increased and this indicates that the coating is slightly affected by the corrosive environment. In other words, by examining the SEM, XRD and PDS values given in Table 4 together, the highest corrosion resistance was found in L_{10} group. The presence of Al detected in the EDX analyses (Fig. 11d) is believed to be contaminated from the alumina-based mortar used for the grinding process during the synthesizing of bioceramic powders. It is understood that the presence of Si comes from the sandblasting process, and it may remain in small amounts on the substrate material despite the cleaning procedure applied before the coatings. Also, the presence of Na is probably due to sodium hydroxide, which is used as a pH regulator in the production of bioceramic powders. However, because these elements are too small in quantity and partially biocompatible, they would not have a detrimental effect on living cells.

5. CONCLUSIONS

In order to enhance the corrosion resistance and adhesion strength, Boron (B) powders have been doped into HA with varying amounts (5, 10, and 15 wt %) using the simple acid-base chemical process. The synthesized B–HA bioceramic powders was coated on 316L implants and sintered by using electrophoretic deposition (EPD) as alternative applications in orthopaedics. The significant findings can be summarized as below:

- Compared to the only-HA coatings, the increased Boron addition increased the bonding between the B and HA powders and provided a crack-free surface morphologies providing higher adhesion. The highest adhesion was determined in the 15 wt % B–HA coatings as 25.8 MPa was measured for the 90 s.

- The boron addition increased the deposited weight and so coating thickness on the 316L substrates

coated by the EPD method by depending on the coating time and applied voltage, e.g. the 5, 10, and 15 wt % B–HA bioceramic coatings provided higher film thicknesses than the only-HA coatings.

— Iodine used in the EPD coating suspension revealed better charging of the bioceramic powder particles in the suspension, thus facilitating the coating and providing homogeneous coating surfaces.

— Among different sintering applications, the optimal sintering conditions were determined at 750°C sintering temperature and 5°C min⁻¹ sintering rate, and the optimum sintering was found to have positive effect on adhesion.

— Throughout the in vitro corrosion tests, the coatings of 15 wt % B–HA (Group L₁₀) provided the best corrosion resistance compared to the uncoated and other coating groups, only-HA, 5 and 10 wt % B–HA).

REFERENCES

- Williams, D.F., *J. Mater. Sci.*, 1987, vol. 22, no. 10, pp. 3421–3445.
- Burny, F., Donkerwolcke, M., and Muster, D., *Mater. Sci. Eng., A*, 1995, vol. 199, no. 1, pp. 53–59. [https://doi.org/10.1016/0921-5093\(95\)09907-7](https://doi.org/10.1016/0921-5093(95)09907-7)
- Hsu, R.W.W., Yang, C.C., Huang, C.A., and Chen, Y.S., *Mater. Chem. Phys.*, 2005, vol. 93, nos. 2–3, pp. 531–538. <https://doi.org/10.1016/j.matchemphys.2005.04.007>
- Say, Y. and Aksakal, B., *J. Mater. Res. Technol.*, 2020, vol. 9, no. 2, 1742–1749.
- Aksakal, B., Say, Y., Buyukpinar, Ç., and Bakirdere, S., *Ceram. Int.*, 2017, vol. 43, pp. 12609–12615.
- Bronzino, J.D., *Biomedical Engineering Handbook*, Boca Raton, FL: CRC Press, 2000.
- Bogdanoviciene, I., Beganskiene, A., Tonsuaadu, K., Glaser, J., Meyer, H.J., and Kareiva, A., *Mater. Res. Bull.*, 2006, vol. 41, pp. 1754–1762.
- Murugan, R. and Ramakrishna, S., *Compos. Sci. Technol.*, 2005, vol. 65, pp. 2385–2406.
- Aksakal, B. and Demirel, M., *Proc. Inst. Mech. Eng., Part H*, 2018, vol. 232, no. 10, pp. 1039–1047.
- Barheine, S., Hayakawa, S., Jäger, C., Shirotsaki, Y., and Osaka, A., *J. Am. Ceram. Soc.*, 2011, vol. 94, no. 8, pp. 2656–2662.
- Ong, J.L. and Chan, D.C., *Crit. Rev. Biomed. Eng.*, 2000, vol. 28, nos. 5–6, pp. 28–35.
- Aksakal, B., Kom, M., Tosun, H.B., and Demirel, M., *Eur. J. Orthop. Surg. Traumatol.*, 2014, vol. 24, no. 5, pp. 813–819.
- Say, Y., Aksakal, B., and Dikici, B., *Ceram. Int.*, 2016, vol. 42, no. 8, pp. 10151–10158.
- Say, Y. and Aksakal, B., *J. Mater. Sci.: Mater. Med.*, 2016, vol. 27, no. 6, p. 105.
- Mavrogenis, A., Dimitriou, R., Parvizi, J., and Babis, G., *J. Musculoskeletal Neuronal Interact.*, 2009, vol. 9, no. 2, pp. 61–71. <https://doi.org/10.1016/j.joms.2007.05.013>
- Mucalo, M., *Hydroxyapatite (HAp) for Biomedical Applications*, Amsterdam: Woodhead Publ., 2015.
- Hakki, S.S., Bozkurt, B.S., and Hakki, E.E., *J. Trace Elem. Med. Biol.*, 2010, vol. 24, pp. 243–250. <https://doi.org/10.1016/j.jtemb.2010.03.003>
- Ternane, R., Cohen-Adad, M.T., Panczer, G., et al., *J. Alloys Compd.*, 2002, vol. 333, pp. 62–71. [https://doi.org/10.1016/S0925-8388\(01\)01558-4](https://doi.org/10.1016/S0925-8388(01)01558-4)
- Devirian, T.A. and Volpe, S.L., *Crit. Rev. Food Sci. Nutr.*, 2003, vol. 43, no. 2, pp. 219–231. <https://doi.org/10.1080/10408690390826491>
- Yesilbag, D., *J. Uludag Univ. Fac. Vet. Med.*, 2008, vol. 27, nos. 1–2, pp. 61–68. <https://dergipark.org.tr/pub/uluvfd/issue/13525/163617>
- Aksakal, B. and Boccaccini, A.R., *Mater. Lett.*, 2012, vol. 76, pp. 177–180. <https://doi.org/10.1016/j.matlet.2012.02.059>
- Mohseni, E., Zalnezhad, E., and Bushroa, A.R., *Int. J. Adhes. Adhes.*, 2014, vol. 48, pp. 238–257. <https://doi.org/10.1016/j.ijadhadh.2013.09.030>
- Williams, R., *Mater. Today*, 2011, vol. 14, no. 6, p. 290.
- Wennerberg, A., Hallgren, C., Johansson, C., and Danelli, S., *Clin. Oral Implants Res.*, 1998, vol. 9, no. 1, pp. 11–19.
- Tozar, A. and Karahan, I.H., *Surf. Coat. Technol.*, 2018, vol. 340, pp. 167–176.
- Göncü, Y., Geçgin, M., Bakan, F., and Ay, N., *Mater. Sci. Eng., C*, 2017, vol. 79, no. 1, pp. 343–353.
- Kokubo, T. and Takadama, H., *Biomaterials*, 2006, vol. 27, pp. 2907–2915. <https://doi.org/10.1016/j.biomaterials.2006.01.017>
- Papavinasam, S., Boca Raton, FL: CRC Press, 2008, pp. 49–83.
- Albayrak, Ö., *Mater. Charact.*, 2020, vol. 113, pp. 82–89.
- Khoshsima, S., Alshemary, A.Z., Tezcaner, A., Surdem, S., and Evis, Z., *Process. Appl. Ceram.*, 2018, vol. 12, no. 2, pp. 143–152.
- Güler, H., Gündoğmaz, G., Kurtuluş, F., Çelik, G., and Gacanoğlu, Ş.S., *Solid State Sci.*, 2011, vol. 13, pp. 1916–1920. <https://doi.org/10.1016/j.solidstatesciences.2011.08.016>
- Wang, Y.C., Leu, I.C., and Hon, M.H., *J. Am. Ceram. Soc.*, 2004, vol. 87, no. 1, pp. 84–88. <https://doi.org/10.1111/j.1551-2916.2004.00084.x>
- Wei, M., Ruys, A.J., Milthorpe, B.K., Sorrell, C.C., and Evans, J.H., *J. Sol-Gel Sci. Technol.*, 2001, vol. 21, pp. 39–48. <https://doi.org/10.1023/A:1011201414651>
- Askari, N., Yousefpour, M., and Rajabi, M., *J. Aust. Ceram. Soc.*, 2020, vol. 56, pp. 1053–1059.